

Figure 4 An example of sheet-like downwelling flow, showing a temperature isosurface.

heats up, until the stagnant-lid style of convection is reached again (Fig. 1e–f).

This cycle repeated itself several times; this is shown in Fig. 2 where the temporal evolution of the Nusselt number and of the surface toroidal-poloidal kinetic energy ratio is displayed for the whole simulation. The narrow peaks correspond to a failure of the stagnant lid. The subduction process occurs on a timescale that is shorter than the time needed for a new lid to grow to its full thickness, which is about an order of magnitude larger for this simulation. This is indicated in Fig. 2, where the subduction process stops at point e and the subducted lid is replaced at point f. The formation of ridges did not only occur near the boundaries of the box, as one might expect looking at Fig. 1, but also in the middle of the box. During the simulation, the lid subducted usually by parts, but we have also seen one event of an almost complete resurfacing.

Our experiment shows several features related to plate tectonics as currently observed. The rheology produces plate-like regions with very little internal strain, fairly sharp changes in velocity at plate boundaries, downwelling flow that is sheet-like, and regularly occurring trench migration. The surface toroidal-poloidal kinetic energy ratio is significant, but it is low compared with that of the Earth. Including a mechanism of self-lubrication into the rheology^{12,13} may increase this ratio. Further, the Earth does not currently exhibit tectonic activity with a strong episodic character. The process of subduction followed by a long period of growth of a new stagnant lid is more similar to the process that is active on Venus²⁴. When the lid fails, in the current model, it is removed much faster by subduction than it can be replaced by new material that is cooled from the top. This episodic behaviour would not occur when the rate of disappearance and the rate of replacement of the lid are the same. Then one would obtain a continuous process consisting of failure, subduction and replacement taking place simultaneously. Such a process is believed to be active on Earth.

We note that our model is still simple, and that many features—such as phase boundaries, internal heating and the presence of chemically buoyant continents—are not included. Our model needs to be modified by including ‘memory’ into the rheology as plate boundaries may continue to exist even when they are not active. Including these effects could bring the behaviour of our model closer to plate tectonics as it is observed on Earth. Our calculations, however, do show that an appropriate rheology translates the internal dynamics into plate-like surface motion. In our view, this is an important step towards a unifying model of mantle convection and plate tectonics. □

Received 8 September 1997; accepted 14 July 1998.

1. Gable, C. W., O’Connell, R. J. & Travis, B. J. Convection in three dimensions with surface plates: Generation of toroidal flow. *J. Geophys. Res.* **96**, 8391–8405 (1991).
2. Hager, B. H. & O’Connell, R. J. A simple global model of plate dynamics and mantle convection. *J. Geophys. Res.* **86**, 4843–4867 (1981).
3. Olson, P. & Corcos, G. M. A boundary layer model for mantle convection with surface plates. *Geophys. J. R. Astron. Soc.* **62**, 195–219 (1980).

4. Weinstein, S. A. & Olson, P. Thermal convection with non-Newtonian plates. *Geophys. J. Int.* **111**, 515–530 (1992).
5. Ribe, N. M. The dynamics of thin shells with variable viscosity and the origin of toroidal flow in the mantle. *Geophys. J. Int.* **110**, 537–552 (1992).
6. Davies, G. F. Mantle convection model with a dynamic plate: Topography, heat flow and gravity anomalies. *Geophys. J. Int.* **98**, 461–464 (1989).
7. Gurnis, M. Large-scale mantle convection and the aggregation and dispersal of supercontinents. *Nature* **332**, 695–699 (1988).
8. King, S. D. & Hager, B. H. The relationship between the plate velocity and trench viscosity in Newtonian and power law subduction of calculations. *Geophys. Res. Lett.* **17**, 2409–2412 (1990).
9. Schmeling, H. & Jacoby, W. R. On modelling the lithosphere in mantle convection with non-linear rheology. *J. Geophys.* **50**, 89–100 (1981).
10. Zhong, S. & Gurnis, M. Towards a realistic simulation of plate margins in mantle convection. *Geophys. Res. Lett.* **22**, 981–984 (1995).
11. Zhong, S. & Gurnis, M. Interaction of weak faults and non-Newtonian rheology produces plate tectonics in a 3D model of mantle flow. *Nature* **383**, 245–247 (1996).
12. Bercovici, D. A simple model of plate generation from mantle flow. *Geophys. J. Int.* **114**, 635–650 (1993).
13. Bercovici, D. Plate generation in a simple model of lithosphere-mantle flow with dynamic self-lubrication. *Earth. Planet. Sci. Lett.* **144**, 41–51 (1996).
14. Christensen, U. Convection in a variable viscosity fluid: Newtonian versus power law. *Earth. Planet. Sci. Lett.* **64**, 153–162 (1983).
15. Christensen, U. & Harder, H. 3D convection with variable viscosity. *Geophys. J. Int.* **104**, 213–226 (1991).
16. Čadež, O., Richard, Y., Martinec, Z. & Matyska, C. Comparison between Newtonian and non-Newtonian flow driven by internal loads. *Geophys. J. Int.* **112**, 103–114 (1993).
17. Nataf, H. C. & Richter, F. M. Convection experiments in fluids with highly temperature dependent viscosity and the thermal evolution of the Earth. *Phys. Earth Planet. Inter.* **29**, 320–329 (1982).
18. Solomatov, V. S. Scaling of temperature-dependent and stress-dependent viscosity convection. *Phys. Fluids* **7**, 266–274 (1995).
19. Stengel, K. C., Oliver, D. C. & Booker, J. R. Onset of convection in variable-viscosity fluid. *J. Fluid Mech.* **120**, 411–431 (1982).
20. Fowler, A. C. Boundary layer theory and subduction. *J. Geophys. Res.* **98**, 21997–22005 (1993).
21. Trompert, R. A. & Hansen, U. The application of a finite volume multigrid method to 3D flow problems in a highly viscous fluid with a variable viscosity. *Geophys. Astrophys. Fluid Dyn.* **83**, 261–291 (1996).
22. Trompert, R. A. & Hansen, U. On the Rayleigh number dependence of convection with a strongly temperature-dependent viscosity. *Phys. Fluids* **10**, 351–360 (1998).
23. Burgess, S. L. & Wilson, S. D. R. Spin-coating of a viscoplastic material. *Phys. Fluids* **8**, 2291–2297 (1996).
24. Head, J. W. Venus after the flood. *Nature* **372**, 729–730 (1994).

Acknowledgements. We thank D. Bercovici and C. W. Gable for comments and suggestions, and the Dutch national computing facilities foundation (NCF) for computer time on a Cray C916. This work was supported by the Dutch National Science Foundation NWO.

Correspondence and requests for materials should be addressed to U.H. (e-mail: hansen@earth.uni-muenster.de).

Two-dimensional matches from one-dimensional stimulus components in human stereopsis

Bart Farell

Institute for Sensory Research, Syracuse University, Syracuse, New York 13244-5290, USA
Center for Vision Research, SUNY Health Science Center, Syracuse, New York 13210-2375, USA

Three-dimensional visual scenes project onto the retina of the eye as two-dimensional images. The third dimension, depth, is projected as subtle differences between left and right retinal images. As early as the 1830s, stereoscopic depth perception was shown to depend on horizontal disparities between these images¹. To detect disparity, the visual system must match corresponding parts of the two retinal images. To identify the stimulus elements used in stereo matching, I applied a disparity-adaptation technique to visual patterns whose one-dimensional components and two-dimensional features have very different disparities. Surprisingly, the adaptors that are effective in altering depth perception appear widely separated in depth from the patterns they adapt. I conclude that stereo matching occurs in all directions of two-dimensional space and that one-dimensional components are the stimulus primitives, the fundamental elements of stereo matching. This is a reversal of the classical view of stereo correspondence as a one-

dimensional (horizontal) matching of monocular two-dimensional features²⁻⁴.

Figure 1a shows a stereogram containing a horizontally offset line and a zero-disparity occluder. When the half-images are fused (by crossing one's eyes), the line is revealed to be behind the plane of fixation, just as if no occluder were present. However, the superimposed half-images (Fig. 1b) show a variety of local disparity directions between the segments of the occluder, including horizontal, vertical and oblique directions. These 'aperture disparities' have a well-known analogue in motion perception⁵, but are absent from the non-overlapping stimuli typically used to study stereopsis. Thus, in naturalistic, 'layered' scenes of occluding and transparent surfaces, stereo correspondence becomes a two-dimensional (2D) matching problem in which horizontal disparity is not a reliable cue to depth. This dissociation of retinal disparity and perceived depth can be exploited to identify the stimulus primitives of human stereopsis.

Here I use 'stereo plaids', the simplest frequency-domain 2D stereo stimuli, which are made by superimposing two sinusoidal gratings (Fig. 1c). Unlike broad-band, sharp-edged patterns (Fig. 1a), sinusoidal stereo plaids do not segregate in depth, even if their components have very different disparities. Instead, they cohere in depth, forming a 2D pattern within a single depth plane^{6,7}. The disparities of stereo plaids are, like aperture disparities, generally non-horizontal. Depth coherence has a familiar one-dimensional (1D) analogue in the perception of a squarewave grating (alternating light and dark stripes) or similar broadband pattern. One sees a unified grating at the depth corresponding to the disparity of the fundamental, despite the differing disparities of the higher harmonics. The simplest explanation is that the visual system matches edges of the squarewave—and 2D features of plaids—not the harmonics.

To identify the matching primitives, it is necessary first to determine how the perceived depth of a plaid is related to the disparities of its components. I presented superimposed gratings

orientated at 15° and 45° to observers, who classified the resulting plaids as 'near' or 'far' with respect to the plane of fixation. The disparity of one grating was zero and that of the other, expressed as a phase angle, ranged over $\pm\pi/4$. Stimuli appeared briefly, to preclude eye movements that could alter the disparities. When the 15° grating had zero disparity, the plaid was seen as 'near' if the 45° grating had negative disparity and as 'far' if it had positive disparity. However, when the 45° grating had zero disparity, the plaid was seen with reversed depth: as 'far' if the disparity of the 15° grating was negative and as 'near' if it was positive (Fig. 2). It is clear that relative depth is not predictable from component disparities alone (and that depth coherence is not depth capture⁸ or disparity averaging⁹).

What does predict the depth judgements of Fig. 2 is the horizontal component of the disparity of the plaids' 2D features (for example, intersections or 'blobs'). This is given by $\rho \cos(\phi)$ for direction ϕ and magnitude ρ of the 2D feature disparity, where

$$\phi = \theta_1 - \arctan \left\{ \frac{\Delta_1 \cos(\theta_2 - \theta_1) - \Delta_2}{\Delta_1 \sin(\theta_2 - \theta_1)} \right\} \quad (1)$$

$$\rho = \left| \frac{\Delta_1}{\cos(\phi - \theta_1)} \right| \quad (2)$$

θ_1 and θ_2 are the gratings' disparity directions measured normal to their orientations, and Δ_1 (non-zero) and Δ_2 are the respective disparity amplitudes. So, depending on grating orientation, the disparities of the 2D features can be similar to, or very different from, the disparities of the component gratings. This is why adding a zero-disparity grating to a 'far' grating can yield a depth-reversed 'near' plaid.

There would seem to be little risk in concluding that the matching primitives are some set of 2D stimulus features. This hypothesis is supported by the association between the polarity (near compared with far) of perceived depth and the direction (negative compared with positive) of the horizontal component of the 2D feature

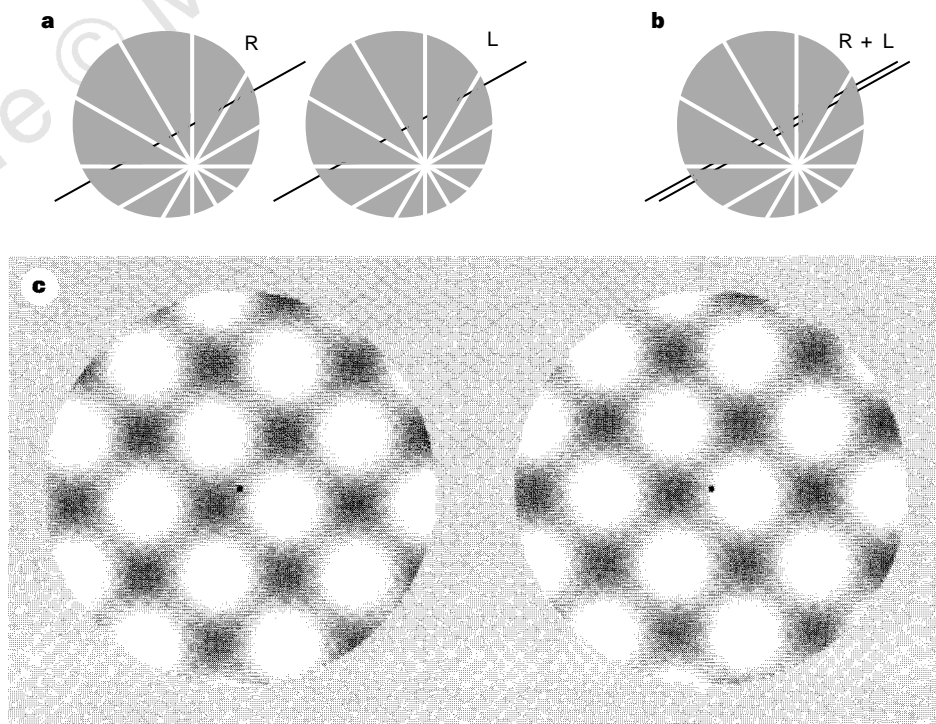


Figure 1 Stereograms. **a**, When cross-fused, the line, with positive horizontal disparity, appears behind the zero-disparity occluder. **b**, Superimposed half-images show that the line's local disparities are not confined to the horizontal meridian, but run parallel to the apertures between segments of the occluder. **c**, Stereo plaid composed of gratings with positive and zero disparity. The plaid's

2D feature disparities parallel the zero-disparity grating (135°), just as the local disparities in **a** parallel the apertures of the zero-disparity occluder. The two gratings appear at the same depth, forming a coherent plaid; observers cannot determine which grating has zero disparity.

disparity, and the lack of such an association involving the 1D component disparity (Fig. 2). In fact, however, 1D primitives cannot be excluded at this point. Next I examine and test these alternatives, taking advantage of the large disparity difference between 2D features and 1D components in depth-reversed stereo plaids.

In traditional theories, features of the 2D image are matched horizontally. However, developments such as aperture disparities, the perceived depth data of Fig. 2, and results of other studies^{10,11} show that stereo matching is not confined to the horizontal meridian or epipolar lines. A model for extracting the disparities of these features without incurring the full cost of an unconstrained 2D search uses arbitrarily oriented receptive fields (Fig. 3a). These sample left and right retinal images with a disparity direction that is normal to the orientation of the receptive field. Data must be pooled across orientations to overcome the stereo aperture problem, that is, a 1D detector cannot reliably code a 2D disparity. A pair of symmetrically oriented receptive fields yields an efficient pooling algorithm (Fig. 3a).

Under an alternative hypothesis, 1D components are the matching primitives (Fig. 3b). Physiologically realistic receptive fields such as those of Fig. 3a can be used to register matches between local 1D Fourier components of the left and right retinal images in the first of two processing stages (Fig. 3b). First-stage neural responses are combined at a second stage to compute the disparities of 2D features by implementing equations (1) and (2). The model unifies the stereo processing of 1D and 2D stimuli, matching 1D components in order to compute the 2D disparity field that the one-stage model (Fig. 3a) extracts directly. The model's second stage can also facilitate the difficult problem of perceiving transparency by selectively combining components within, but not between, broadband patterns (for example, squarewave gratings in Fig. 2). A related two-stage model of motion perception has been productive and controversial for the past 15 years¹².

These models code disparity in a 2D correspondence space and use the full range of receptive-field orientations, not just the vertical¹³ or the unorientated^{4,27}. In this respect, the receptive-field organization of both models differs significantly from models that have been proposed previously for coding the disparity of 2D stimuli. Each receptive field has its disparity direction normal to its preferred orientation and thus performs an efficient 1D match.

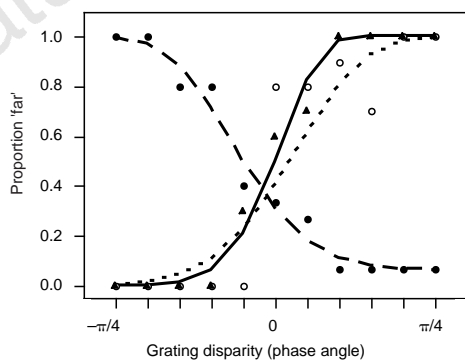


Figure 2 Perceived depth polarity of stereo plaids as a function of disparity of one component grating; the other component had zero disparity. Grating orientations were 15° and 45°. Data are for one observer; the other two observers gave similar results. Triangles, solid line: 45° grating had disparity given on abscissa. Gratings were sinusoidal and cohered in depth. Filled circles, dashed line: 15° grating had disparity given on abscissa. Gratings were sinusoidal and cohered, but now the psychometric function is reversed. Open circles, dotted line: same as filled circles, except that the gratings were squarewaves. These gratings segregate in depth; the data describe depth of the 15° grating. Depth reversal thus depends on the coherence of the gratings, and therefore on 2D stimulus structure. Lines are based on Weibull fits.

Yet disparity coding across receptive fields is fully 2D in that the correspondence search spans all directions and can establish a match in any direction. The models differ in their stereo primitives and also in their relation to feature detection. In the one-stage model, the detection of 2D monocular features occurs before stereo matching; in the two-stage model, stereo matching precedes feature detection. However, in the limiting case of a single point-like stimulus as input, the two models are indistinguishable.

Thus, we can specify the disparities of stereo plaids, and those of other 2D patterns, either as 2D feature disparities or as 1D component disparities. But which does the visual system actually use? To find an answer, I used an adaptation method. After prolonged viewing of an adapting stimulus, a spatially similar test stimulus with a neighbouring disparity appears displaced in depth away from the adaptor¹⁴. I used this displacement after-effect to enhance the discriminability of test stimuli whose disparities flank the disparity of the adaptor. Observers selected the farther of two depth-reversed plaids that differed slightly in depth (Fig. 4). If the visual system extracts the disparity of 2D features, then depth discrimination should be facilitated by adapting to disparity d_2 (adaptor A in Fig. 4), midway between the 2D feature disparities of the two plaids. If the visual system extracts the disparity of 1D components, then facilitation should result from adapting to disparity d_1 (adaptor B), midway between the 1D component disparities.

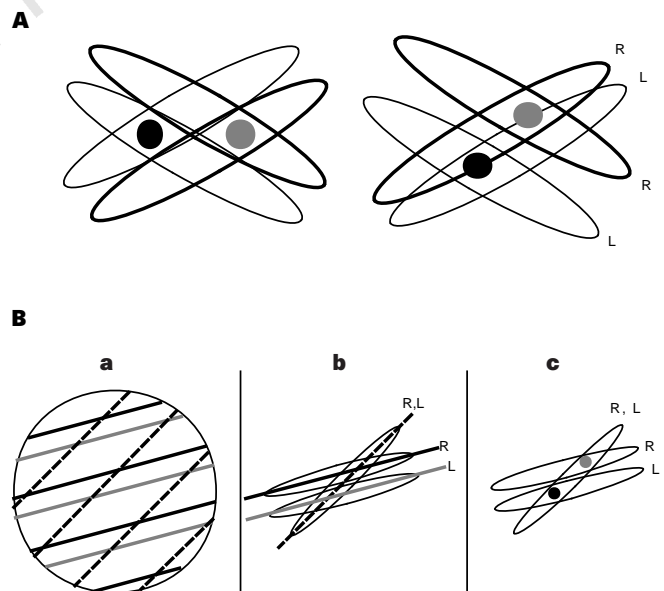


Figure 3 One- and two-stage models of stereo matching. **A**, One-stage model for coding 2D feature disparities. Receptive fields are tuned to disparities that are perpendicular to their orientations. Two such receptive fields (here showing similar spatial frequency preferences) with arbitrary orientations θ and $-\theta$ form the basic computational unit. The stimuli (disks) have horizontal (left) and oblique (right) disparities. Horizontal and vertical disparities are recoverable from the sum and difference of phase shifts, respectively: $D_H = (\phi_1 + \phi_2)(\lambda/4\pi)/\sin\theta$; $D_V = (\phi_1 - \phi_2)(\lambda/4\pi)/\cos\theta$, where ϕ_1 and ϕ_2 are the separate phase shifts and λ is the receptive-field period. **B**, Two-stage model for deriving 2D feature disparities from 1D components. **a**, A reversed-depth stereo plaid containing a 45° zero-disparity grating. **b**, First-stage coding of disparities of 1D components by neurons with elongated receptive fields. Neurons are activated to the extent that their binocular receptive fields match Fourier components of the stimulus; activation is highest for the receptive field profiles shown here. **c**, Second-stage combination of active units, implementing equations (1) and (2) to compute intersections of the receptive fields. The output is a computed disparity of 2D features (disks), the same disparity that the one-stage model codes directly (**A**, right). Note that the receptive-field disparity and the 2D feature disparity have horizontal components of opposite signs. L and R denote left and right eyes.

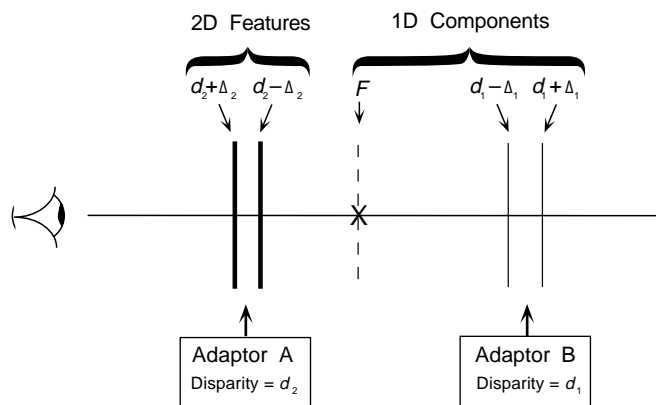


Figure 4 Adaptation experiment. Two reversed-depth stereo plaids appear in separate intervals on each trial. Observers select the interval containing the more distant of the plaids, that is, the one with disparity $d_2 - \Delta_2$. Task performance was measured before and after observers adapted to a grating or plaid whose disparity lay either between the disparities of the 2D features appearing in the two intervals (adaptor A), or between the non-zero disparities of the component gratings (adaptor B). Observers see the test stimuli as plaids in front of the fixation plane.

Figure 5 compares pre- and post-adaptation performance. Neither grating adaptors nor plaid adaptors significantly improve discrimination ($P > 0.05$) when the adapting disparity is centred between the disparities of the 2D features of the test plaids (A adaptors). However, both grating adaptors and plaid adaptors significantly improve discrimination when the adapting disparity is centred between the disparities of the 1D components (B adaptors), provided that the 1D components of adapting and test patterns are parallel. The probability of correct discrimination increased to 80% from the pre-adaptation level of 69%. Adaptors that were oriented orthogonally had no significant effect on performance. Additional conditions in which adaptors had disparities midway between disparities of the test plaids' second-order gratings¹⁵ also showed no effect. Thus, adaptation is effective at the disparity of the test plaids' 1D components, in the direction normal to these components. This occurs even though the test stimuli are not seen at the 'far' depth of the effective adaptors, but rather at the 'near' depth corresponding to the disparity of the 2D features. The results, which are predicted by the two-stage model and run counter to other models of stereo matching, implicate 1D components as the primitives of a 2D stereo correspondence process.

The visual system's use of vertical as well as horizontal disparities has been hinted at ever since von Helmholtz's observations¹⁶. A few past studies have shown that, in some conditions, naturalistic vertical disparities can influence perceived depth^{17,18}. The present results take this further, indicating that stereo matching is intrinsically a 2D correspondence process. First, disparities can have any direction during aperture viewing. Second, the two-stage model codes the stereo correspondence of 2D stimuli in two dimensions, regardless of the direction of the stimulus disparity. For example, a point stimulus whose retinal disparity is strictly horizontal would match binocular receptive fields having every correspondence direction; the correspondence would have non-zero disparity in every direction except the strictly vertical. This results from matches between elongated receptive fields and the point's isotropically distributed 1D components. It also helps to explain a long-standing physiological puzzle. Most visual cortical neurons are binocularly sensitive¹⁹⁻²², but they do not respond selectively to horizontal disparities only. Instead, they respond to any of a variety of disparity directions. The distribution is isotropic²³⁻²⁵, or very nearly so²⁶. This

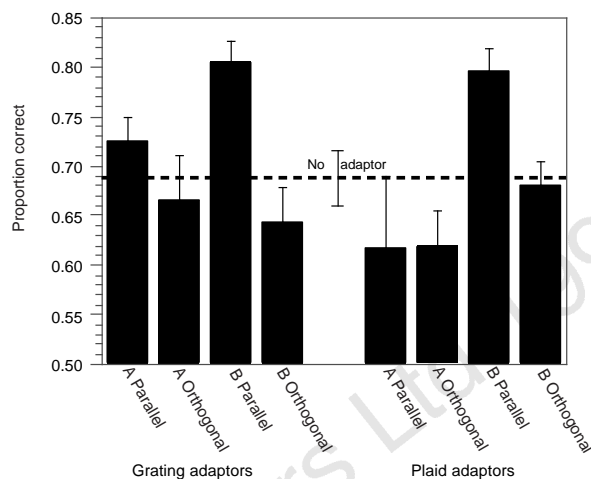


Figure 5 Depth discrimination performance. Data for one observer; the data for two other observers were similar. Chance performance is 50%. 'A' adaptors have disparities centred between those of the test patterns' 2D features (Fig. 4). 'B' adaptors have disparities centred between those of the test patterns' 1D components. Discriminability is significantly enhanced ($P < 0.05$ by Newman-Keuls tests) relative to the no-adaptation performance only for 'B' adaptors with 1D components that are parallel to those of test plaids. Systematically varying the adaptor disparity within the vicinity of the disparity of the 2D test features uncovered no region of improved discriminability; included within this region were the horizontal disparities of the test plaids' second-order gratings. Bars represent 1 s.e.m.

has long seemed oddly mismatched to the disparities of isolated objects, which have a much greater range in the horizontal than in the vertical direction. It has been suggested that the isotropy of disparity tuning serves merely to maintain ocular vergence, but it can instead be seen as an evolutionary response to the demands of stereoscopic matching in a layered (for example, arboreal) environment. □

Methods

Stimuli. In all experiments, visual patterns were constructed from achromatic sinusoidal gratings (or, in one case, squarewave gratings) with a spatial frequency of 1.0 cycle per deg and a Michelson contrast of 5 or 10%. Background luminance was 39 cd m⁻². The patterns appeared with the requisite disparity in two circular windows, one for each eye, and were viewed through a mirror stereoscope at a distance of 57 cm. A black square, 6 min on a side, was continually present at the centre of each window, as a zero-disparity fixation point. A random phase shift was added to each grating on each trial, with corresponding left- and right-eye gratings receiving the same shift, to prevent the possible learning of monocular position cues. A Macintosh computer controlled the stimulus display.

Perceived depth experiment. (See Fig. 2.) On each trial, a single pair of superimposed gratings appeared for 180 ms, with abrupt onset and offset. The contrast of each grating was 5%. Waveforms were sinusoidal in two conditions and square in a third condition. The gratings had orientations of 15° and 45° and appeared in a circular window with a diameter of 7.85° of visual angle. One of the gratings had zero disparity throughout a run of 55 trials; the other grating was given a disparity randomly selected on each trial from 11 alternative values within a phase range of $\pm \pi/4$. Observers clicked on one of two on-screen buttons, displayed 0.5 s after stimulus offset, to indicate whether the plaid (or squarewave grating) was 'near' or 'far', relative to the plane of fixation. Trials were self-paced; no feedback about accuracy of responses was given. Each data point was based on 30 trials. Three observers participated; their monocular and stereo acuities were normal or corrected-to-normal. One observer was naive as to the purposes of the experiment.

Adaptation experiment. (See Figs 4 and 5.) On each trial, two reversed-depth

stereo plaids appeared in separate 180-ms intervals separated by a 400-ms blank period. Observers selected the interval containing the more distant of the two test plaids. The plaids consisted of a 15° positive-disparity grating and a 45° zero-disparity grating, each with 5% contrast. They appeared at slightly different depths on the near side of the plane of fixation, as shown in Fig. 4. The two 15° gratings had disparity phase angles of 31.0° and 18.6°, yielding a horizontal disparity difference of 8'. The disparity of the adapting pattern was either midway between the disparities of the 15° component gratings appearing in the two test intervals or midway between the disparities of the 2D features appearing in the two test intervals. There were four adapting stimuli: a 15° grating, a 105° grating, a plaid with components at 15° and 45°, and a plaid with components at 105° and 135°. The horizontal disparities of the adaptors were set to correspond to the depths of adaptors A and B in Fig. 4. For plaid adaptors, both components (and the 2D features) had the same horizontal spatial disparity. Adapting gratings had spatial frequencies of 1.0 cycle per deg, the same as the test gratings; they appeared in a circular window with a diameter of 9°, to ensure complete retinal overlay of the 7.85° test window. Each run of 20 trials began with an adapting period of 40 s, and each trial began with a 4 s 'topping-off' adaptation period, with 0.4 s separating adaptor offset and the first test interval. Adaptors underwent smooth harmonic motion at 1.0 cycle per s to minimize retinal adaptation. Adaptation and no-adaptation conditions were identical except for the adaptor grating contrast (10 and 0%, respectively). Adaptor contrast and duration were identified by systematic sampling to favour disparity adaptation at the expense of contrast adaptation; relatively brief and low-contrast adaptors tended to yield this result. Contrast adaptation and disparity adaptation have opposite expected consequences, the former inhibiting and the latter facilitating depth discrimination. Observers were instructed to maintain fixation on the central square throughout each trial and to respond by clicking one of two on-screen buttons to indicate the interval containing the test plaid more distant from the observer. Of three observers, one was naive; all had corrected-to-normal monocular and stereo acuities. Each data point was based on 40 trials.

Received 21 November 1997; accepted 31 July 1998.

1. Wheatstone, C. Contributions to the physiology of vision. Part the first. On some remarkable, and hitherto unobserved, phenomena of binocular vision. *Phil. Trans. R. Soc. Lond. B* 2, 371–393 (1838).
2. Ogle, K. N. *Researches in Binocular Vision* (Saunders, Philadelphia, 1950).
3. Bishop, P. O. *Neurosciences Research Study Program Boulder Symposium* (ed. Schmitt, F. O.) (Rockefeller Univ. Press, New York, 1970).
4. Julesz, B. *Foundations of Cyclopean Perception* (Univ. of Chicago Press, 1971).
5. Wallach, H. *On Perception* (ed. Wallach, H.) (Quadrangle, New York, 1976).
6. Farell, B. & Ahuja, S. Binocular disparity of 1- and 2-D contours. *Invest. Ophthalmol. Vis. Sci.* (suppl.) 37, 284 (1996).
7. Farell, B. Depth coherence and depth reversal in stereo plaids. *Invest. Ophthalmol. Vis. Sci.* (suppl.) 38, 904 (1997).
8. Ramachandran, V. S. & Cavanagh, P. Subjective contours capture stereopsis. *Nature* 317, 527–531 (1985).
9. Schumer, R. A. & Ganz, L. Disparity averaging in random dot stereopsis. *J. Opt. Soc. Am.* 69, 1479 (1979).
10. Stevenson, S. B. & Schor, C. M. Human stereo matching is not restricted to epipolar lines. *Vision Res.* 37, 2717–2723 (1997).
11. Morgan, M. J. & Castet, E. The aperture problem in stereopsis. *Vision Res.* 39, 2737–2744 (1997).
12. Adelson, E. H. & Movshon, J. A. Phenomenal coherence of moving visual patterns. *Nature* 300, 523–525 (1982).
13. DeAngelis, G. C., Ohzawa, I. & Freeman, R. D. Depth is encoded in the visual cortex by a specialized receptive field structure. *Nature* 352, 156–159 (1991).
14. Blakemore, C. & Hague, B. Evidence for disparity detecting neurons in the human visual system. *J. Physiol. (Lond.)* 225, 437–455 (1972).
15. Hibbard, P. B. & Langley, K. Plaid slant and inclination thresholds can be predicted from components. *Vision Res.* 38, 1073–1084 (1998).
16. von Helmholtz, H. *Treatise on Physiological Optics* Vol. 3 (ed. Southall, J. P. C.) (translated from German 3rd edn) (Optical Society of America, 1925).
17. Gillam, B., Chambers, D. & Lawergren, B. The role of vertical disparity in the scaling of stereoscopic depth perception: an empirical and theoretical study. *Percept. Psychophys.* 44, 473–483 (1988).
18. Rogers, B. J. & Bradshaw, M. F. Vertical disparities, differential perspective and binocular stereopsis. *Nature* 361, 253–255 (1993).
19. Hubel, D. H. & Wiesel, T. N. Receptive fields, binocular interaction and functional architecture in the cat's visual cortex. *J. Physiol. (Lond.)* 160, 106–154 (1962).
20. Barlow, H. B., Blakemore, C. & Pettigrew, J. D. The neural mechanism of binocular depth discrimination. *J. Physiol. (Lond.)* 193, 327–342 (1967).
21. Poggio, G. F. & Fischer, B. Binocular interaction and depth sensitivity in striate and prestriate cortex of behaving rhesus monkey. *J. Neurophysiol.* 40, 1392–1405 (1977).
22. Zeki, S. Functional specialization and binocular interaction in the visual areas of rhesus monkey prestriate cortex. *Proc. R. Soc. Lond. B* 204, 379–397 (1979).
23. Ferster, D. A comparison of binocular depth mechanisms in area 17 and 18 of the cat visual cortex. *J. Physiol. (Lond.)* 311, 623–655 (1981).
24. LeVay, S. & Voigt, T. Ocular dominance and disparity coding in cat visual cortex. *Vis. Neurosci.* 1, 395–414 (1988).
25. Nikara, T., Bishop, P. O. & Pettigrew, J. D. Analysis of retinal correspondence by studying receptive fields of binocular single units in cat striate cortex. *Exp. Brain Res.* 5, 353–372 (1968).

26. Anzai, A., Ohzawa, I. & Freeman, R. D. Neural mechanisms underlying binocular fusion and stereopsis: Position vs. phase. *Proc. Natl Acad. Sci. USA* 94, 5438–5443 (1997).
27. Mayhew, J. E. W. & Frisby, J. P. Stereopsis masking in humans is not orientationally tuned. *Perception* 7, 431–436 (1978).

Acknowledgements. I thank D. C. Moore for laboratory assistance, and S. Ahuja, R. van Ee, J. Krauskopf, D. Matza, D. G. Pelli and S. B. Stevenson for comments and discussion.

Correspondence and requests for materials should be addressed to B.F. (e-mail: bart_farell@isr.syr.edu).

Who reads temporal information contained across synchronized and oscillatory spike trains?

Katrina MacLeod, Alex Bäcker & Gilles Laurent

California Institute of Technology, Division of Biology 139-74, Pasadena, California 91125, USA

Our inferences about brain mechanisms underlying perception rely on whether it is possible for the brain to 'reconstruct' a stimulus from the information contained in the spike trains from many neurons^{1–5}. How the brain actually accomplishes this reconstruction remains largely unknown. Oscillatory and synchronized activities in the brain of mammals have been correlated with distinct behavioural states or the execution of complex cognitive tasks^{6–11} and are proposed to participate in the 'binding' of individual features into more complex percepts^{12–14}. But if synchronization is indeed relevant, what senses it? In insects, oscillatory synchronized activity in the early olfactory system seems to be necessary for fine odour discrimination¹⁵ and enables the encoding of information about a stimulus in spike times relative to the oscillatory 'clock'¹⁶. Here we study the decoding of these coherent oscillatory signals. We identify a population of neurons downstream from the odour-activated, synchronized neuronal assemblies. These downstream neurons show odour responses whose specificity is degraded when their inputs are desynchronized. This degradation of selectivity consists of the appearance of responses to new odours and a loss of discrimination of spike trains evoked by different odours. Such loss of information is never observed in the upstream neurons whose activity is desynchronized. These results indicate that information encoded in time across ensembles of neurons converges onto single neurons downstream in the pathway.

The function of oscillations and synchronization in information processing, perception and action is difficult to establish directly. Studies in mammals have correlated the degree of neural synchronization with specific behavioural or cognitive tasks, such as segmentation⁸, rivalry⁹, and sensorimotor tasks^{10,11}, suggesting a functional link. In locusts, stimulation by odours evokes synchronized firing in dynamic and odour-specific ensembles of projection neurons in the antennal lobe, a region analogous to the vertebrate olfactory bulb^{16–18}. This synchronization relies critically on fast GABA (γ -aminobutyric acid)-mediated inhibition, and can be selectively blocked by local injection of the GABA receptor antagonist picrotoxin¹⁹. Picrotoxin spares the slow modulation of individual projection neuron responses¹⁹ but desynchronizes the firing of the odour-activated assemblies¹⁹ and impairs fine odour discrimination¹⁵. These results establish a causal link between synchronization and perception. They do not, however, determine where information is lost when projection neurons—the information channels—are desynchronized. One possibility is that no single neuron between sensory and motor/cognitive areas is, on its own, sensitive to input synchronization. The behavioural deficit caused